Truncated Gamma Drop Size Distribution Models for Rain Attenuation in Singapore

Lakshmi Sutha Kumar, Yee Hui Lee, *Member, IEEE*, and Jin Teong Ong, *Member, IEEE*

***Abstract*—A model that is less sensitive to errors in the extreme small and large drop diameters, the gamma model with central moments (3, 4 and 6), is proposed to model the rain drop size distribution of Singapore. This is because, the rain rate estimated using measured drop size distribution shows that the contributions of lower drop diameters are small as compared to the central drop diameters. This is expected since the sensitivity of the Joss distrometer degrades for small drop diameters. The lower drop diameters are therefore removed from the drop size data and the gamma model is redesigned for its moments. The effects of the removal of a particular rain drop size diameter on the specific rain attenuation (in dB) and the slant-path rain attenuation calculations with forward scattering coefficients for vertical polarization are analyzed at Ku-band, Ka-band and Q-band frequencies. It is concluded that the sensitivity of the Joss distrometer although affects the rain rate estimation at low rain rates, does not affect the slant path rain attenuation on microwave links. Therefore, the small drop diameters can be ignored completely for slant path rain attenuation calculations in the tropical region of Singapore.**

***Index Terms*—dead-time problem, drop diameters, gamma distributions, rain, rain attenuation, rain drop size distribution.**

I. Introduction

RAIN drop size distribution model is required for the evaluation of microwave propagation attenuation due to rain. The prediction of rain attenuation is very important to communication engineers since the microwave attenuation caused by rain limits the performance of the microwave link. Rain attenuation is much more severe in the tropical and equatorial regions due to higher precipitation rates. In the design of both terrestrial and earth-satellite communication links, detailed knowledge of the drop size distribution (DSD) becomes imperative for the calculation of the rain-induced attenuation.

In 1943, Laws and Parsons examined the relationship between raindrop size and rain intensity [1]. For a long time, the exponential DSD has been the most widely used analytical parameterization for the raindrop size distribution:

$$N(D) = N_0 \exp(-\Lambda D) \tag{1}$$

where $N(D)$ is the number of drops per unit volume per unit interval of drop diameter D and the parameters N_o and Λ can be determined experimentally. Marshall and Palmer [2] suggested that $N_0 = 8000\ \mathrm{m}^{-3}\ \mathrm{mm}^{-1}$ and $\Lambda = 4.1R^{0.21}\ \mathrm{mm}^{-1}$ where R is the rainfall rate in mm/hr. However, subsequent DSD measurements have shown that the exponential distribution does not capture rain DSDs and a more general function is necessary.

Although some authors [3] have considered using a lognormal distribution, Ulbrich [4] and Willis [5] have suggested that the DSD is best modeled by a gamma distribution (which has the exponential distribution as a special case) though Smith [6] recently has argued that the exponential distribution is preferred because of its simplicity. In this paper, the use of the gamma distribution for modeling the DSD in the tropical and equatorial regions will be examined. Before considering how best to estimate the parameters of a gamma DSD, we need to understand the limitations of the Joss distrometer (JWD), which is the instrument used to measure DSD in this study.

JWD tends to underestimate the number of small drops during a heavy rain event because of ringing of the Styrofoam cone when it is hit by the rain drops. This is known as the distrometers' dead time. To correct for it, the correction matrix, supplied by the manufacturer is used [7]. In the presence of numerous large rain drops during intense tropical rain events of $\mathrm{R} \geq 20$ mm/hr, drop sizes smaller than 1.0 mm are underrepresented [8]. This problem is due to an automatic threshold circuitry that monitors the ambient noise level to reject spurious pulses. However, under intense rain, the high noise level of the drops themselves is interpreted as ambient noise and small-drop signals are rejected. The larger drops produce longer dead times and therefore, requires greater correction. However, if there are no drops in a given bin, the correction matrix does not add any drops to the bin. Rather, it modifies the DSD and increases the high moments of the drop size such as rain rate significantly. This is a problem of the correction matrix, and thus, many users choose not to implement it [8], [9]. At the largest drop size end, drops larger than 5.0–5.5 mm in diameter cannot be resolved at their true size; rather, they are assigned to the largest size bin. The sensitivity degradation of the JWD has been discussed in the comparative studies carried out between the JWD and other drop size measurement instruments in [7] and [10].

In the present study, the dead-time correction has been applied using the software provided by Distromet, Inc. The correction is intended to correct up to 10% of the accuracy. The distrometer was installed on the rooftop of a 50 m high building where the environmental noise is minimal.

The DSD over Singapore was studied previously by Li *et al.* [11] and Ong and Shan [12], [13]. Li *et al.* [11], Ong and Shan [12] have proposed a modified gamma model for DSD. In [13], they modeled the rain drop size distributions by the lognormal model. In their paper, Singapore lognormal and gamma models

Manuscript received January 23, 2009; revised September 11, 2009; accepted October 18, 2009. Date of publication February 02, 2010; date of current version April 07, 2010.

L. S. Kumar and Y. H. Lee are with Nanyang Technological University, Singapore 639798, Singapore (e-mail: laks0008@ntu.edu.sg; eyhlee@ntu.edu.sg).

J. T. Ong is with C2N Pte. Ltd, Singapore 199098, Singapore (e-mail: jtong@c2n-ap.com).

Digital Object Identifier 10.1109/TAP.2010.2042027

are compared with the results from different regions in [13]. In both the papers [12], [13], the 0^{th}, 1^{st} and 2^{nd} nd moments and the 0^{th}, 2^{nd} and 3^{rd} moments are used to represent the modified gamma model. However, for the distrometer data, the use of the 0^{th} moment is impossible and the use of the 1st moment is not advisable, since the number of drops with diameters less than $\mathrm{D}_{\min}$ is not known [14]. Many authors [6], [8], [9], [15], [16] prefer to work with central moments, since JWD has degraded sensitivity at small drop diameters. Kozu and Nakamura [15], and Tokay and Short [8] used the 3^{rd}, 4^{th} and 6^{th} moments (MM346). Smith [6], [16] suggested 2^{nd}, 3^{rd} and 4^{th} moments to model gamma DSD (MM234). Ulbrich and Atlas [17] took into account the maximum value for drop diameters, $\mathrm{D}_{\max}$, and used the 2^{nd}, 4^{th} and 6^{th} moments (MM246). Their method allows for truncation of the DSD at the large diameter end of the spectrum due in part to instrumental effects. Timothy [18] used 3^{rd}, 4^{th} and 6^{th} moments to represent Singapore's DSD using lognormal model. He observed a significant decrease in drop density in small drop bins from visual inspection of Singapore's data (year 1997–1998 data).

In recent years, it has become common for DSD to be represented by a normalized DSD [19], [20]. The normalization allows the shapes of different DSDs from different rain regimes to be compared relative to the total liquid water content and the mean drop size. The concept of normalized gamma distribution was first introduced by Willis [5] and revisited by Illingworth and Blackman [19] in 2002. Normalized gamma DSD has been used by Testud *et al.* [20]. Generally normalization is used to remove the dependence of N_0 and Λ in the gamma DSD, allowing comparison of the shape of the distributions at different rainfall rates.

Caracciolo [9] used the higher order moments 4^{th}, 5^{th} and 6^{th} to form a gamma model (MM456) which is less sensitive to small drop diameters. She selected these moments because the higher moments are less dependent on small drops which are underestimated by Joss distrometer due to dead time problem. This model is especially effective at higher rain rates, where the dead time effect is severe. Smith [16] pointed out that the bias is stronger when higher order moments are used. Brawn [14] compared the gamma models using different combinations of moments (MM346, MM234, MM246 and MM456) along with his new procedure. He found that MM456 model deviates more from the measured data compared to the gamma models using lower moment combinations, MM234, MM246 and MM346. This conclusion is similar to Smith's [16]. But a model which is less sensitive to small drop diameters is required as stated by Caracciolo [9]. Therefore, Brawn [14] suggested that an interesting alternative to develop a less sensitive model is by completely ignoring the counts in the lower order bins.

This research work started with the modeling of rain drop size distribution in the tropical region using different models, such as lognormal, gamma and exponential models. The three mentioned models describe the larger drop diameters well. However, the exponential model tends to overestimate the smaller drop diameters whereas the gamma and the lognormal models follow the distrometers' measured DSD at the smaller drop diameters. Since the measured DSD experiences the dead time effect at the smaller drop diameters, the accurate modeling of the small drop diameters needs to be carefully examined. Therefore, by taking Brawn's recommendation to ignore the counts in the lower order bins, the gamma model can be used as a universal model including the tropical region of Singapore.

In this paper an investigation is performed to study the validity of ignoring the counts in the lower order bin as proposed by Brawn for rain attenuation calculations. This is done by removing the small drop size bins consecutively starting from the first bin and redesigning the gamma models using the remaining bins for each bin removal. The deviations in the redesigned gamma models as compared to the actual gamma model are studied. This will aid in the understanding of the importance of small rain drop sizes to the rain attenuation of the terrestrial and earth-satellite communication links. Based on these redesigned models, the importance of small rain drop sizes on communication links at different frequencies is examined.

II. Methodology

The measurement of rain drop size distribution has been conducted since August 1994 at the Nanyang Technological University (1°21′N, 103°41′E), Singapore (NTU). The rain data is collected from August 1994 to September 1995, excluding June and July 1995 using a "Joss-type" Distrometer RD-69. Rain rates are calculated from measured DSD for seven rain rates, 1.96 mm/hr, 4.20 mm/hr, 10.45 mm/hr, 22.80 mm/hr, 66.54 mm/hr, 120.30 mm/hr and 141.27 mm/hr.

The Joss distrometer has an integration time of one minute, therefore, rain rate calculated from the distrometers' measured data is directly used. The contribution of individual bins is found in order to check the effect of the dead time problem at different rain rates. In our previous work [21], gamma model is used to find the contribution of individual bins and it is reported that the error in rain rate calculations from the removal of drop diameters below 0.77 mm is small as compared to the removal of the larger drop diameters.

In this paper, the DSD is described by a three-parameter gamma distribution. The 3^{rd}, 4^{th} and 6^{th} moments are proposed to model gamma DSD (MM346) in Singapore as suggested by Kozu and Nakamura [15]. In order to form a gamma DSD model which is less sensitive to small drop diameters, consecutive bins are removed, meaning; initially, only bin 1 is removed, and then bins 1 and 2 are removed, followed by the removal of bins 1 to 3 and bins 1 to 4 starting from the smallest drop size diameter. Moments are calculated from the remaining bins in each case. In this way, four different truncated gamma models are designed. Mean square errors are calculated to compare the modeled DSDs with the measured drop size distribution.

The study continues by examining the contribution of particular rain drops on the specific rain attenuation of microwave signals using forward scattering coefficients for a vertically polarized wave at frequencies 11 GHz, 28 GHz, 38 GHz and 48 GHz. T-Matrix code is used to calculate the forward scattering coefficients which are more accurate over various drop shapes and radio frequencies.

The Ku-band frequency of 11 GHz [18], representative of the INTELSAT 602 satellite and the Ka-band frequency of 28 GHz [22], representative of the IPSTAR satellite is used in this study. A number of sources [23] have identified 38 GHz

TABLE I
THRESHOLDS OF DROP SIZE BINS AND MEASURED RAIN DROPS FROM JWD AT SEVEN RAIN RATES

bin i	Lower bound D_{il} (mm)	Upper bound D_{iu} (mm)	Mean value D_i (mm)	Date : 26-02-1995 / Time (min) 1934	1801	1747	1856	1846	1828	1711
				Rain rate (mm/hr) 1.96	4.20	10.45	22.80	66.54	120.30	141.27
1	0.31	0.41	0.36	2	5	5	X	X	X	X
2	0.41	0.51	0.46	8	35	26	26	23	X	X
3	0.51	0.60	0.55	38	36	43	59	62	7	X
4	0.60	0.72	0.66	68	55	66	50	144	31	5
5	0.72	0.83	0.77	49	41	52	56	123	49	23
6	0.83	1.00	0.91	88	87	99	88	253	169	112
7	1.00	1.23	1.12	72	100	158	110	364	446	308
8	1.23	1.43	1.33	24	63	72	114	260	342	277
9	1.43	1.58	1.51	9	29	41	75	145	231	217
10	1.58	1.75	1.67	2	17	40	89	176	311	214
11	1.75	2.08	1.91		6	67	148	236	471	417
12	2.08	2.44	2.26		3	24	63	168	315	347
13	2.44	2.73	2.58		1	3	20	86	157	168
14	2.73	3.01	2.87			1	10	37	86	91
15	3.01	3.39	3.20				1	41	56	89
16	3.39	3.70	3.54				1	7	20	52
17	3.70	4.13	3.92					3	5	30
18	4.13	4.57	4.35					1	6	4
19	4.57	5.15	4.86						0	1
20	>5.15		5.30						1	1

X-No rain drops in measured data

as the largest growth area in the supply of fixed radio-relay systems as lower frequency bands become congested. The 48 GHz [24] band has been allocated world-wide for fixed service with High Altitude Platform Stations (HAPS). The main drawback in HAPS is the troposphere effects on the propagation, particularly rain attenuation that may limit the link availability. Therefore, in the Q-band, 38 GHz and 48 GHz are selected for this study.

Slant-path rain attenuation A_1 exceeding 1% of the time is calculated using ITU-R P.618-9 recommendations [25] for all the truncated gamma models at 11 GHz, 28 GHz, 38 GHz and 48 GHz. The first step in applying this method is to obtain the rainfall intensity for the area of interest, integrated over one minute, which is exceeded for 0.01% of the time.

The averaged $R_{0.01}$ of 122 mm/hr is used in [26] for the NTU site from year 1990 to 1996. $R_{0.01}$ is 126.65 mm/hr for the year 2000, 105.58 mm/hr for 2005 to 2006 and 111.18 mm/hr for 2007 to 2008 also at NTU site. Therefore, 120.30 mm/hr is taken as the $R_{0.01}$ in this paper since it is one of the rain rates considered. Slant-path rain attenuation A_1 exceeding 1% of the time is calculated for all the four frequencies at this rain rate.

Changes in slant-path rain attenuations are calculated by comparing bins removed MM346 gamma models with the actual gamma model. This paper presents the contribution of drop size on specific rain attenuation for different frequencies. The changes in gamma models due to the truncation of lower bins are analyzed along with slant-path rain attenuation calculations. The results from this analysis are useful for the prediction of rain attenuation at Ku-band, Ka-band and Q-band communication links in the tropical region.

III. DATA ANALYSIS AND MEASUREMENT

A. Measured DSD

The Distrometer is capable of measuring the drop diameters ranging from 0.3 mm to >5 mm with an accuracy of ±5%. It distinguishes between drops with time interval of about 1 ms. The total number of drops with diameters ranging from 0.3 mm to >5 mm is divided into 20 different bins for 1 minute integration time [27].

It is possible to calculate the rain rate from the measured number of drops for a minute. Seven different minutes are selected from the rain events that occurred on 26th February 1995. The measured drop counts at different bins from the JWD for those seven minutes are listed along with the thresholds for the drop size bins in Table I.

As can be seen in Table I, as the rain rate increases, the dead time problem can be observed from the lack of drops in the lower bins (labeled as "X"). This will be analyzed in detail in the results section. The diameter D_i is a representative diameter for the ith bin. Generally, the mean value of range is calculated in (2).

$$D_i = D_{il} + \frac{D_{iu} - D_{il}}{2} = D_{il} + \frac{\Delta D_i}{2} \tag{2}$$

where D_{il} and D_{iu} are the lower and upper diameter value of that ith bin respectively. The representative diameter is used

for computing DSD, rain rate and specific rain attenuation. The number of raindrops, n_i, in the ith bin with diameters, D_i, in the range of $D_i \pm \Delta D_i/2$ are collected over a sample area of $S = 5000$ mm^2 with an integration time of $T = 60$ sec determined by the JWD.

The rain rate (in mm/hr) can be calculated from the measured data by

$$R = \frac{3600\pi}{6ST} \sum_{i=1}^{20} D_i^3 n_i. \tag{3}$$

The measured rain drop size distribution $N(D_i)$ (m^{-3} mm^{-1}) [12] can be expressed by

$$N(D_i) = \frac{n_i \times 10^6}{v(D_i) \times S \times T \times \Delta D_i} \tag{4}$$

where $v(D_i)$ is the terminal velocity of rain drop in m/s from Gunn and Kinzer [28].

B. Gamma Modeled DSD

Gamma model is usually expressed in the form

$$N(D_i) = N_0 D_i^{\mu} e^{-\Lambda D_i} \tag{5}$$

where $N(D_i)$ is the number of rain drops per cubic meter per millimeter diameter (m^{-3} mm^{-1}), D_i is the rain drop diameter (mm), N_0, μ and Λ are parameters to be determined through the measured DSD. The estimates from the method of moments are obtained by equating a sufficient number of measured moments to the corresponding theoretical moments. The kth experimental moment is expressed by M_k

$$M_k = \frac{N_t}{n} \sum_{i=1}^{n} D_i^k \tag{6}$$

where n is the number of samples and N_t is the particle number concentration and is equal to M_0; M_k is obtained through the experimental data.

The kth theoretical moments can be written as

$$\Omega_k = \int_0^{\infty} D^k N(D) dD \tag{7}$$

By equating the theoretical and experimental moments, it is derived that

$$M_k = \frac{N_0}{\Lambda^{\mu+k+1}} \Gamma(\mu + k + 1). \tag{8}$$

Using $k_1 = 3, k_2 = 4$ and $k_3 = 6$, the gamma DSD parameters are obtained [15] as follows:

$$\mu = \frac{11F - 8 + \sqrt{F(F+8)}}{2(1-F)} \text{ with } F = \frac{M_4^3}{M_3^2 M_6} \tag{9}$$

$$\Lambda = (\mu + 4) M_3 / M_4 \tag{10}$$

$$N_0 = \Lambda^{\mu+4} M_3 / \Gamma(\mu + 4). \tag{11}$$

C. Specific Rain Attenuation

Specific attenuation due to a rain path depends on the rain rate, shape of the rain drops, distribution of the rain drops size, operating frequency and wave polarization. The scattering calculations were performed using the T-Matrix method [29] which enables the computation of the complex forward scattering coefficients, considering spherical drops at 20°C with the shape according to the Pruppacher-Pitter model [30] for H and V polarizations. The specific rain attenuation for H and V polarizations γ_H and γ_V in dB/km are given by

$$\gamma_{H,V} = 8.686 \times 10^3 \times \lambda \times \sum_{i=1}^{20} \mathrm{Im}(f_{H,V}(D_i)) N(D_i) dD_i \tag{12}$$

where $f_H(D_i)$ and $f_V(D_i)$ are complex forward scattering coefficients (in units of m) for horizontal and vertical polarization respectively, $N(D_i)$ is the number of drops per unit volume per unit drop diameter in m^{-3} mm^{-1}, dD_i is the drop size interval in mm and λ is the wavelength.

D. The ITU-R Rain Attenuation Model

The ITU-R P.618-9 [25] gives a step by step procedure to estimate the long-term statistics of the slant-path rain attenuation at a given location for frequencies up to 55 GHz. The earth station is assumed to be at the rooftop of a building in NTU, Singapore at location (1°21′N, 103°41′E) and the earth station height is measured using a Symmetricom XL-GPS receiver. The rain height h_R is calculated in (13) using the 0° isotherm height data h_0, given by ITU-R P.839-3 [31]

$$h_R = h_0 + 0.36 \text{ [km]} \tag{13}$$

The elevation angle, θ, is considered from 10° to 90° in steps of 10°. The trend of slant path rain attenuation is not similar at different frequencies as the elevation angle changes. High Altitude Platform Stations [32] use the full range of elevation angles for their different coverage zones (urban, suburban and rural area coverage). Therefore, different elevation angles are considered in order to study the variations in slant-path rain attenuation at the four frequencies.

The effective slant path length L_E is then calculated as explained in ITU-R P.618-9 (refer to [25] for details) using the earth station height above mean sea level h_s (km), elevation angle θ, latitude φ and the rain height h_0. Using the effective slant path length, L_E and the calculated γ_R in (12), the attenuation exceeding 0.01% of the year $A_{0.01}$ is calculated as

$$A_{0.01} = \gamma_R L_E \text{ [dB]} \tag{14}$$

The estimated attenuation to be exceeded for other p percentages of an average year, in the range 0.001% to 5%, is determined from the attenuation to be exceeded for 0.01% for an average year using (15)

$$A_p = A_{0.01} \left(\frac{p}{0.01} \right)^{-(0.655 + 0.033 \ln(p) - 0.045 \ln(A_{0.01}) - \beta(1-p)\sin\theta)} \tag{15}$$

where $\beta = 0$ when $p \geq 1\%$ in this study.

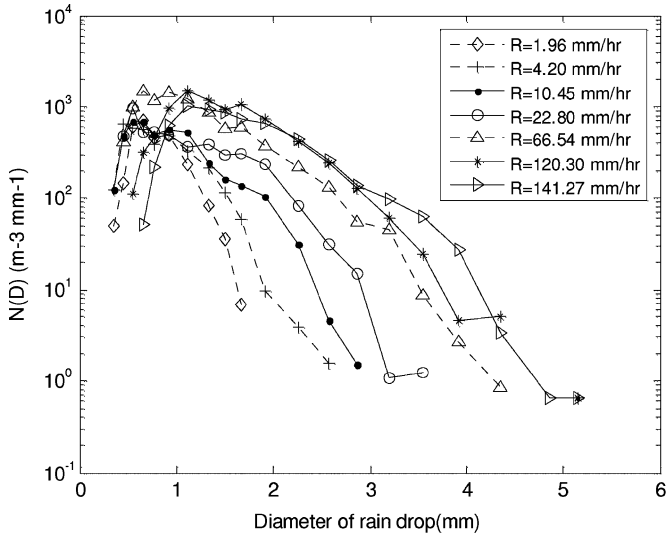

Fig. 1. Drop size distribution for seven rain rates.

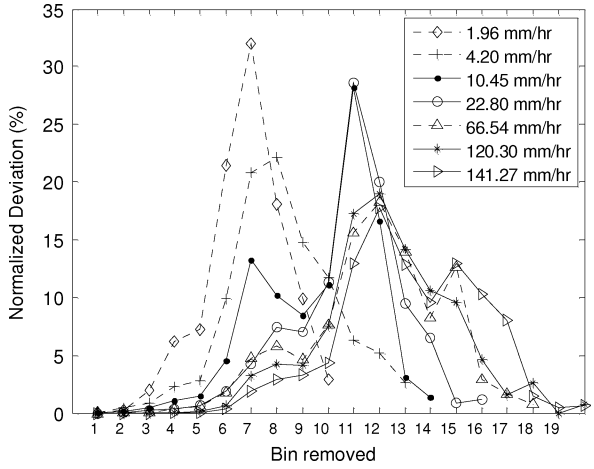

Fig. 2. Normalized deviation (%) for each individual bin removal.

IV. Results

A. Rain Rate and DSD

1) Analysis of Measured DSD: Fig. 1 illustrates the DSD obtained from the measured data using (4) for seven one minute rain rates 1.96 mm/hr, 4.20 mm/hr, 10.45 mm/hr, 22.80 mm/hr, 66.54 mm/hr, 120.30 mm/hr and 141.27 mm/hr. Logarithmic scale is used to represent $N(D_i)$ in the vertical axis. The DSD increases initially with the diameter of the rain drop and then decreases for all the rain rates.

The sensitivity of the distrometer at different bins can be checked by the number of rain drops in the measured data at different rain rates. The lower bins which are marked as "X" in Table I have no rain drops in the measured data. It is clear that the number of lower bins which are affected by dead time problem increase with rain rate. There are zero rain drops in the first bin at 22.80 mm/hr and 66.54 mm/hr and in the first two bins at 120.30 mm/hr.

It is also observed that the first three bins shows low number of counts compared to the higher bins at all the rain rates even after the dead time correction is applied. At 141.27 mm/hr, there are no rain drops in the first 3 bins and only five rain drops at the 4th bin. However, common amongst all rain rates is that, the fifth bin always has a reasonable number of rain drop counts. As stated in the introduction, the numbers of rain drops in the lower 4 bins are severely affected by the dead time problem at high rain rates. In order to study the significance of lower bins which are more erroneous due to the dead time problem, the rain rate estimation is taken. The contribution of individual bins in rain rate estimation is found using measured data in the following section.

2) Contribution of Individual Drop Diameters: The rain rates are calculated using (3) from the measured DSD. Then the rain rate contribution of individual bin is removed one by one, starting from the first bin to the last bin (containing rain drops) for the measured DSD. The rain rate with individual bins removed is calculated for each case. The difference between the measured rain rate and the rain rate with the jth bin removed is then calculated in order to study the significance of individual bins with its corresponding range of rain drop size diameters. This will provide information on the importance and contribution of each drop diameter range to the overall rain rate.

The normalized deviation (%) is calculated using the true rain rate and the rain rate with the jth bin removed using the following equation

$$ND_j(\%) = \frac{[R(\text{true}) - R(j^{\text{th}}\,\text{bin removed})]}{R(\text{true})} \times 100 \quad (16)$$

where $R(\text{true})$ is found from (3) and $R(j\text{th } \textit{bin removed})$ is also found from (3) but with $i = j$th term removed from the summation.

Fig. 2 shows a normalized deviation (%) using (16) for each bin removal at the seven rain rates considered. As seen from Fig. 2, the contribution of bins in rain rate measurement increases gradually with the removal of bin 1 to the middle bins and then decreases for all rain rates. As the rain rate increases, the bin that has the major contribution increases. Therefore, it is clear that at higher rain rates, the contribution of larger drops is more significant in rain rate estimation as is expected.

At the lower rain rate of 4.20 mm/hr, from Table I, the highest number of rain drop count appears at bin 7 ($D_i = 1.12$ mm), however, the most significant bin in rain rate estimation is bin 8 ($D_i = 1.33$ mm). Even though the highest number of rain drop count appears at bin 7, the most significant bin in rain rate estimation is bin 11 at 10.45 mm/hr. This shows that the contribution of rain drops to the overall rain fall rate is not only dependent on the number of drop counts and drop diameter but also the distribution. At the low rain rate of 1.96 mm/hr, most drop counts are in bin 6, with the number of drop counts distributed between bins 4 to 8 (Table I). The most significant bin at this rain rate is bin 7 (Fig. 2). At the high rain rate of 141.27 mm/hr, the drops are quite equally distributed over bins 6 to 18. This results in a number of bins (above bin 10) showing significant contribution to the overall rain rate. This confirms that the contribution to the overall rain rate is dependent on both the drop diameter and drop count distribution.

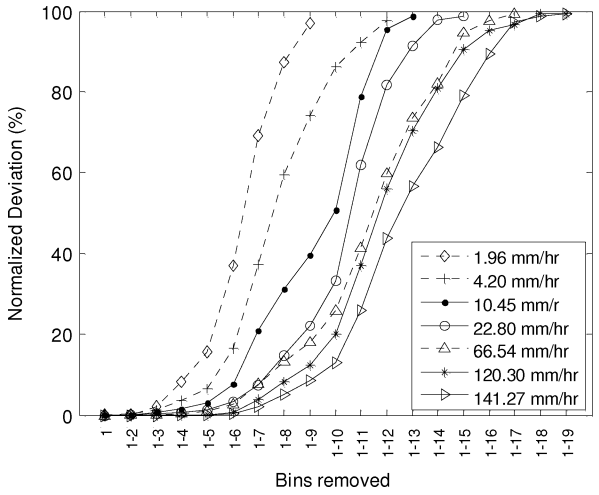

Fig. 3. Normalized deviation (%) for consecutive bins removal.

The ND_j (%) is very small at rain rates from 1.96 mm/hr to 10.45 mm/hr for the first 2 bins. The contributions of 3rd and 4th bins are more significant at these rain rates. The total ND_j (%) produced by the first 4 bins is 8.45, 3.75 and 1.71 at 1.96 mm/hr, 4.20 mm/hr and 10.45 mm/hr respectively. Afterwards, the ND_j (%) increases with the removal of the successive bins. The total normalized deviation produced by the first 4 bins is less than 1% at the higher rain rates from 22.80 mm/hr to 141.27 mm/hr.

In Fig. 3, the percentage of normalized deviation is calculated, but this time, instead of removing one bin at a time, consecutive bins are removed starting from the smallest drop size diameter. This enables us to study the contribution of the range of the rain drop size diameters to the overall rain rate. As expected from Fig. 3, when the number of bins removed increases, the deviation increases correspondingly. The point of this study is to find the bin after which there is a sharp increase in deviation. When the first 1 to 2 bins are removed, the deviation is minimal for all the considered rain rates. However, when bins 1 to 3 are removed, there is a sudden increase in the deviation for rain rates 1.96 mm/hr and 4.20 mm/hr. After that, with the consecutive removal of bins 1 to 4, 1 to 5 and so on, the change in deviation is significant for all the rain rates considered.

This gives a clear indication that the first 2 bins are affected severely by the distrometers' dead time problem at rain rates from 1.96 mm/hr to 10.45 mm/hr. For higher rain rates of 22.80 mm/hr and above, the significant increase in deviation starts from the consecutive removal of bins 1 to 5. Therefore, it is concluded from ND_j (%) calculations that the first two bins can be neglected for lower rain rates ($\leq$ 22.8 mm/hr) and the first 4 bins can be neglected for higher rain rates ($>$22.80 mm/hr).

From the above analysis, it can be assumed that the dead time problem is severe at the lower four bins. Therefore, taking into account of both the lower and higher rain rates, the first four bins are removed consecutively from bin 1 to bin 4 to redesign the gamma models in the following section. These truncated gamma models will be used in the specific rain attenuation and slant-path rain attenuation calculation in the following sections.

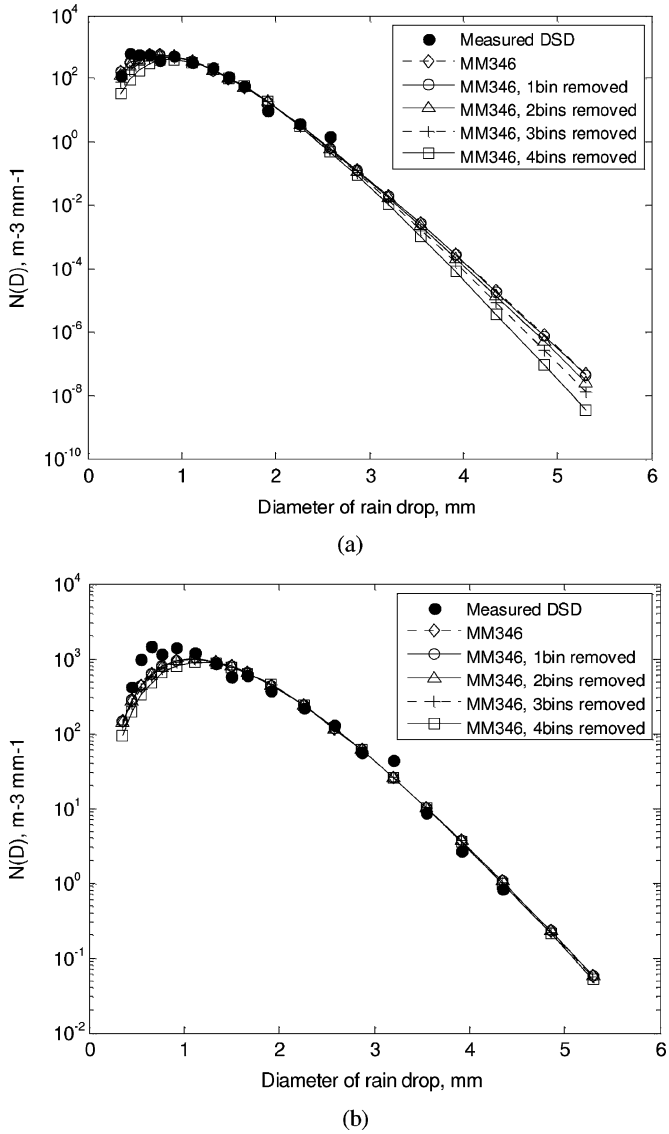

Fig. 4. Truncated gamma models with actual gamma model and measured DSD. (a) 4.20 mm/hr, (b) 66.54 mm/hr.

B. Truncated Gamma Models

In order to obtain the gamma model less sensitive to lower bins; the first bin is removed and the moments are calculated from the remaining bins using (7). Then, the gamma model is redesigned using (9) to (11); next, the first two bins are removed and the moments are calculated using the remaining bins and using these moments the gamma model is redesigned; similarly, gamma models are redesigned for the removal of the first 3 bins and the first 4 bins.

Fig. 4 shows the redesigned gamma models at 4.20 mm/hr and 66.54 mm/hr. From Fig. 4, it can be seen that, in general, all the gamma models fit well with the measured data at both 4.20 mm/hr and 66.54 mm/hr with the exception of one redesigned gamma model. This is where 4 bins are removed before the gamma model is redesigned at the rain rate of 4.20 mm/hr as shown in Fig. 4(a). There is slight deviation at the lower and higher drop diameters. The redesigned gamma models show the same trend as 4.20 mm/hr at the rain rates

TABLE II
MEAN SQUARE ERROR (%) FOR TRUNCATED GAMMA MODELS

MSE (%)					
Rain rate (mm/hr)/ Bins Removed	MM346	1	2	3	4
1.96	1.26	1.30	1.63	7.73	65.95
4.20	3.06	3.10	3.81	5.74	13.52
10.45	6.78	6.95	8.40	12.25	23.49
22.80	24.33	X	26.12	32.11	39.98
66.54	2.89	X	2.99	3.39	4.91
120.30	4.92	X	X	4.90	4.79
141.27	4.43	X	X	X	4.42

1.96 mm/hr, 10.45 mm/hr and 22.80 mm/hr, where the removal of the first 4 bins shows a slight deviation at the lower and higher drop diameters. The deviation at the large diameter end is minimal at 66.54 mm/hr for the 4 bins removed model, however this model also deviates with the measured data at the lower diameters as shown in Fig. 4(b).

All the gamma models fit well with the measured data at 120.30 mm/hr and 141.27 mm/hr at all drop diameters. The accuracy of the gamma models can be evaluated by calculating mean square error as a percentage using the formula

$$\mathrm{MSE}(\%) = \sum_{i=1}^{n} \times \frac{[\log(\text{Measured } N(D_i)) - \log(\text{Modeled } N(D_i))]^2}{n} \times 100 \tag{17}$$

where n is the number of bins in the measured DSD with data. MSE (%) is calculated using (17) for all the rain rates.

Table II shows the MSE (%) for all the rain rates with different number of bins removed. The second column shows the MSE (%) of the actual MM346 model. The cells which are marked as "X" in the Table II have zero rain drops in the measured data. Therefore, the removal of that bins does not change the MSE (%).

From Table II, the removal of bins from 1 to 4 will not make much difference for all the higher rain rates of 66.54 mm/hr and above. At 22.80 mm/hr, from Table II, the MSE (%) of the MM346 gamma model itself is high at 24.33%. This high MSE (%) is because the measured DSD at 22.80 mm/hr deviates more from the gamma model as compared to the DSD at other rain rates, especially at the lower drop size bins. The removal of bins from 1 to 3 increases the MSE from 24.33% for the actual gamma model to 32.11% for the redesigned gamma model, a difference of about 8%. Although the absolute MSE is large, the increase in percentage due to the removal of the bins is similar to that at other rain rates.

For the lower rain rates of 1.96 mm/hr, 4.20 mm/hr and 10.45 mm/hr, the removal of the first 3 and 4 bins introduce higher deviations in MSE (%). It can be concluded that the removal of the first 4 bins with mean drop diameters of less than 0.77 mm can be done for the higher rain rates (>22.80 mm/hr) whereas only lower 2 bins with mean drop diameters less than 0.55 mm can be removed at lower rain rates (≤ 22.80 mm/hr) and yet the accuracy of the redesigned model is not affected. However, for terrestrial and earth-satellite communication links, the contributions of different rain drop diameters at different frequencies are important. The importance of small drop diameters increases at lower rain rates, it is necessary to check their contribution to the rain attenuation calculations especially at high frequencies. This is because, as frequency increases, the drop diameters relative to the wavelength becomes comparable, therefore, the attenuation caused by these small rain drops becomes significant. In the following section, the rain attenuation contribution of the rain drop diameters is studied.

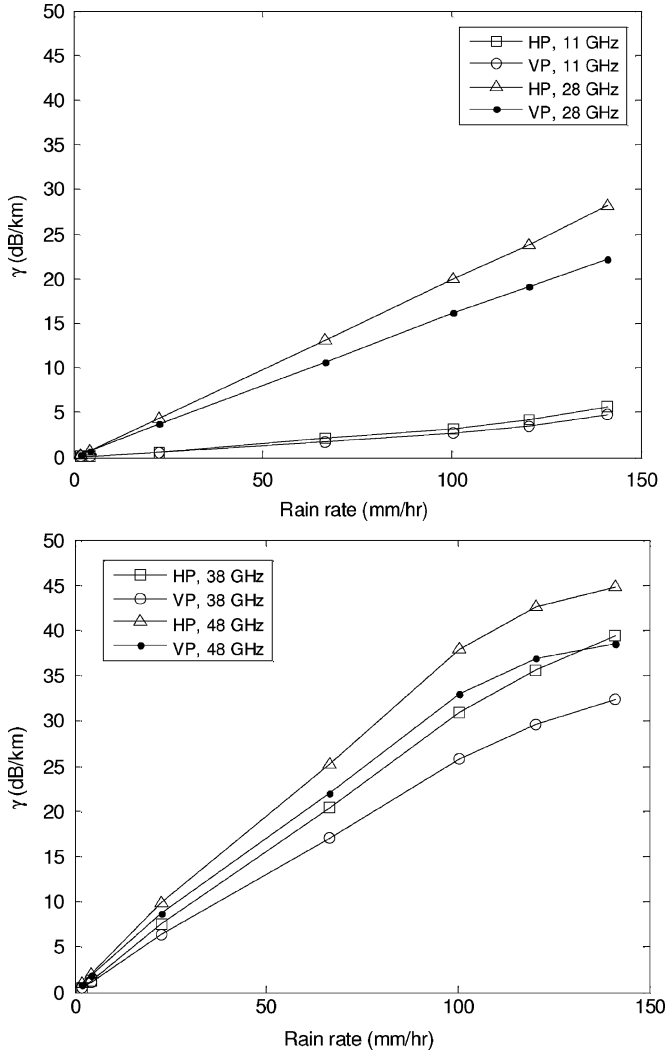

Fig. 5. Specific rain attenuation at different frequencies using gamma model.

C. Specific Rain Attenuation

The specific rain attenuation (in dB/km) is calculated using (12) at different rain rates for the frequencies 11 GHz, 28 GHz, 38 GHz and 48 GHz. Fig. 5 shows the specific attenuation in dB/km at different frequencies for both horizontal and vertical polarization using the MM346 gamma model. The specific rain attenuation increases with both the rain rate and the frequency

TABLE III
SPECIFIC RAIN ATTENUATION (DB/KM) USING FORWARD VERTICAL SCATTERING COEFFICIENTS FOR TRUNCATED GAMMA MODELS

Frequency (GHz)	38					48				
Rain rate (mm/hr)/ Bins Removed	MM346	1	2	3	4	MM346	1	2	3	4
1.96	0.49	0.49	0.49	0.49	0.47	0.84	0.84	0.84	0.83	0.79
4.20	1.14	1.14	1.14	1.14	1.12	1.81	1.81	1.81	1.80	1.77
10.45	2.93	2.93	2.93	2.93	2.91	4.34	4.34	4.33	4.32	4.27
22.80	6.32	X	6.32	6.31	6.29	8.65	X	8.64	8.60	8.55
66.54	17.02	X	17.01	16.99	16.92	21.99	X	21.98	21.93	21.75
120.30	29.54	X	X	29.54	29.52	36.97	X	X	36.96	36.91
141.27	32.40	X	X	X	32.40	38.59	X	X	X	38.58

increase. As seen in Fig. 5, the specific rain attenuation for vertical polarization is smaller than horizontal polarization at all frequencies.

This is because, as the size of the rain drops increase, their shape tends to change from spherical to oblate spheroids. Furthermore [33)], rain drops may also be inclined (canted) to the horizontal because of vertical wind gradients. Thus, the depolarization due to rain can significantly depends on canting and tilt angle with drop vibration effects. The rain induced depolarization has been studied previously [34] by calculating the differential attenuation and the differential phase.

The specific differential attenuation [29] is the difference between the specific rain attenuation for horizontal and vertical polarization and the differential propagation phase is defined as the difference of the imaginary part of the propagation constants of horizontally and vertically polarized waves. The cross-polar discrimination [33] (signal moved to orthogonal polarization/ signal in original polarization) will be different for horizontal and vertical polarization and in absolute value (linear units) will be higher for horizontal polarization (because horizontal polarization will be more attenuated). At low frequencies [34], as expected from the Rayleigh theory, the attenuation and the phase shift is greater in the horizontal polarization compared to the vertical polarization. Therefore, forward scattering coefficients for vertical polarization are used to calculate the specific rain attenuation for the redesigned gamma models.

The specific rain attenuation contributions by individual drop diameters are calculated using vertical forward scattering coefficients at all the rain rates for all the frequencies. Fig. 6 shows the specific rain attenuation contribution of each bin for the four frequencies at 120.30 mm/hr.

It is clear from Fig. 6 that the highest specific rain attenuation contribution moves to lower drop diameters as the frequency increases. Similarly, the highest attenuation contribution of all the other rain rates also moves to lower drop diameters as frequency increases. The smaller wavelengths of higher frequencies are comparable with the rain drop diameters, therefore, results in more attenuation at smaller drop diameters as frequency increases. Small drops tend to be Rayleigh scatterers. Larger drops due to small number and reduced increase of scattering

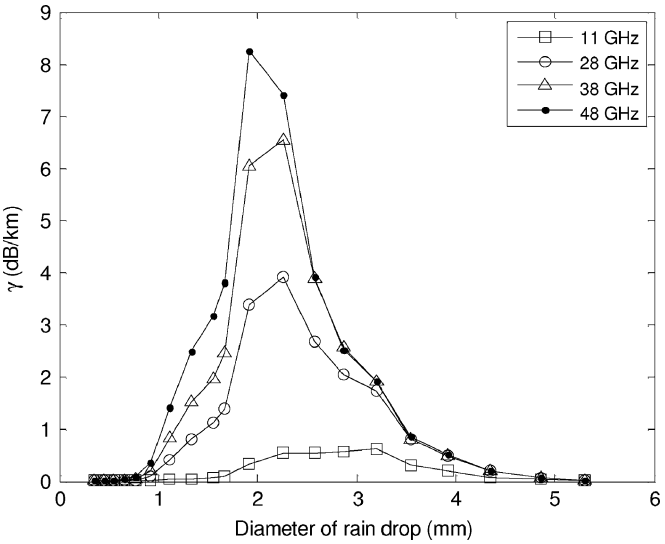

Fig. 6. Specific rain attenuation contributions at different frequencies using gamma model at 120.30 mm/hr.

coefficients become less significant [33]–[35]. Therefore, contribution is so a question of number of drops and wavelength.

Most striking effects of bigger drops at high frequency are the reduction of differential phase that can be observed in depolarization measurements [34], [35]. The reversal in sign of the differential phase at high frequencies is a purely resonance phenomenon in which large drops produce negative differential phase outweighing the positive contribution from smaller ones. Major drops contribute mostly for differential attenuation. As a whole, less deformed smaller drops make a greater relative contribution to the total specific rain attenuation at high frequencies.

Table III shows the calculated specific rain attenuation (dB/km) for the redesigned gamma models with 1, 2, 3 and 4 bins removed using (12) at the Q-band frequencies, 38 GHz and 48 GHz, at 0° elevation angle. Only specific rain attenuation for the Q-band is shown since they have the maximum change in attenuation. The cells which are marked as "X" in Table III have no rain drops in the measured DSD.

The specific rain attenuation increases with both the rain rate and the frequency increase for all the truncated gamma models.

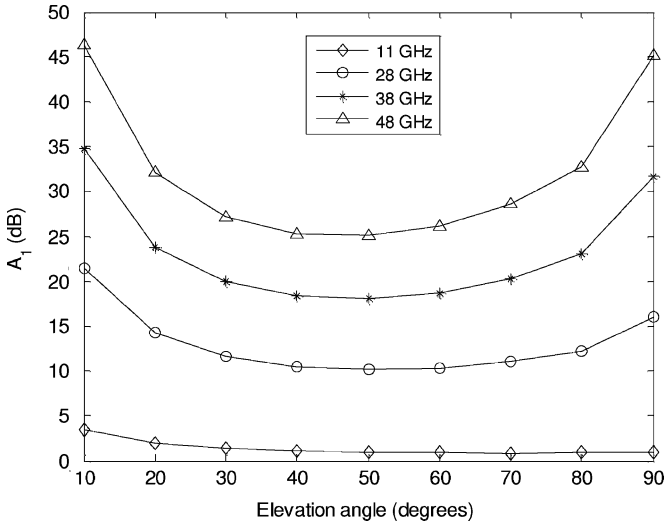

Fig. 7. Slant-path rain attenuation at the four frequencies using gamma model at $R_{0.01}$ (120.30 mm/hr).

The point to note from Table III is that there is not much deviation in attenuation values if any of the lower 4 bins are removed for the redesigned gamma models at any rain rate. Although this change in specific rain attenuation is small, it is worthwhile to evaluate the slant-path rain attenuation values using (15), which are considered next. For slant-path rain attenuation calculations, the specific rain attenuation at different elevation angles are calculated at the four frequencies using forward scattering coefficients for vertically polarized waves for the redesigned gamma models. It is important to note that the specific rain attenuation increases with the increase of elevation angle for vertically polarized waves.

D. Slant-Path Rain Attenuation

The slant-path rain attenuation A_1 (in dB) exceeding 1% of the time is calculated using (13) to (15), with $R_{0.01} = 120.30$ mm/hr, for all the redesigned gamma models at the four frequencies. This is for practical application purposes. From [36], the calculated slant-path rain attenuation (in dB) $A_{0.01}$ exceeding 0.01% of the time and $A_{0.1}$ exceeding 0.1% of the time for a coastal region like Calabar in Nigeria, where the highest average annual accumulation results in a $R_{0.01} = 130$ mm/hr, the $A_{0.01}$ and $A_{0.1}$ are as high as 37.8 dB and 17 dB for 19.45 GHz (Ka-band), and 19.6 dB and 8.4 dB for 12.675 GHz (Ku-band) respectively. These rain attenuation values may exceed the fade margins of practical systems. Similarly, the calculated slant-path rain attenuation values for Singapore at these percentages of time are well above the feasible fade margins especially at high frequencies. Therefore, the slant-path rain attenuation A_1 (in dB) exceeding 1% of the time is selected for the study of the truncated gamma models.

Fig. 7 shows the calculated slant-path rain attenuation using the gamma model at the four frequencies. As frequency increases, slant-path rain attenuation also increases. The increase in elevation angle decreases the slant-path rain attenuation since the slant-path length decreases. This is clear from Fig. 7 that attenuation decreases with the decrease in path length (increase in elevation angle) from the elevation angle 10° to 50° at the three higher frequencies. Above 60°, the slant-path rain attenuation increases again.

The increase in slant-path rain attenuation at higher elevation angles may be due to the presence of convective rain cells [37]. These relatively small cross-sectional areas of intense rain extend from, or often above, the accepted freezing level to the ground. Therefore, the slant-path with the highest elevation will have its entire path virtually through the column of very heavy rain.

In contrast, the slant-path with the lowest elevation due to its long path length may pass through a number of rain cells. However, because the horizontal extent of a cell is relatively small, the total rainfall in the path may be less than those for a higher elevation angle, resulting in less signal attenuation [37]. The calculated slant-path rain attenuation values show that there are insignificant changes for the redesigned gamma models with bins removed from actual gamma model at the four frequencies. The absolute difference between the actual gamma modeled and the redesigned gamma modeled slant-path rain attenuation is calculated by (18)

$$\text{Change in slant} - \text{path rain attenuation} = [A_1(MM346) - A_1(\text{other } ga)] \quad (18)$$

where $A_1(MM346)$ is the slant-path rain attenuation exceeding 1% of time calculated from actual gamma model and A_1 *(other ga)* is the slant-path rain attenuation exceeding 1% of time calculated from redesigned gamma models with bins removed. There are no rain drops in the first two bins at 120 mm/hr; therefore, their slant-path attenuation changes are not plotted.

Fig. 8 shows the slant-path rain attenuation changes for the redesigned gamma models with bins 3 and 4 removed as compared to the actual gamma model at 38 GHz and 48 GHz. As seen in Fig. 8, the changes in slant-path rain attenuation increase at both the frequencies especially at the lower and higher elevation angles for the redesigned gamma models with 4 bins removed from actual gamma model. From Fig. 8(a), it can also be seen that the removal of the first 4 bins results in less than 0.03 dB change in slant-path rain attenuation at 38 GHz. However as shown in Fig. 8(b), at 48 GHz, the removal of the first 4 bins results in a high change in slant-path rain attenuation of around 0.07 dB at the elevation angle of 90°.

This shows that, as frequency increases, the relative contribution from the smaller drop size increases. At 120.30 mm/hr, there are few counts in bin 4; however, as the wavelength of the higher frequency is comparable with the drop diameter, their contribution to the slant-path rain attenuation increases. At the drop diameter 0.66 mm, the drop sizes are one twelfth of λ and one tenth of λ at 38 GHz and 48 GHz respectively.

Since the change in slant-path rain attenuation are below 0.07 dB at all the frequencies for the redesigned gamma model with 4 bins removed, it can be concluded that, since the dynamic range of a satellite system is generally above 1 dB, the removal of the first 4 bins will not affect the satellite communication system for all frequencies within the Ku-band, Ka-band and Q-band. This validates Brawn's recommendations of ignoring the counts in erroneous bins and the truncated gamma models can be used for

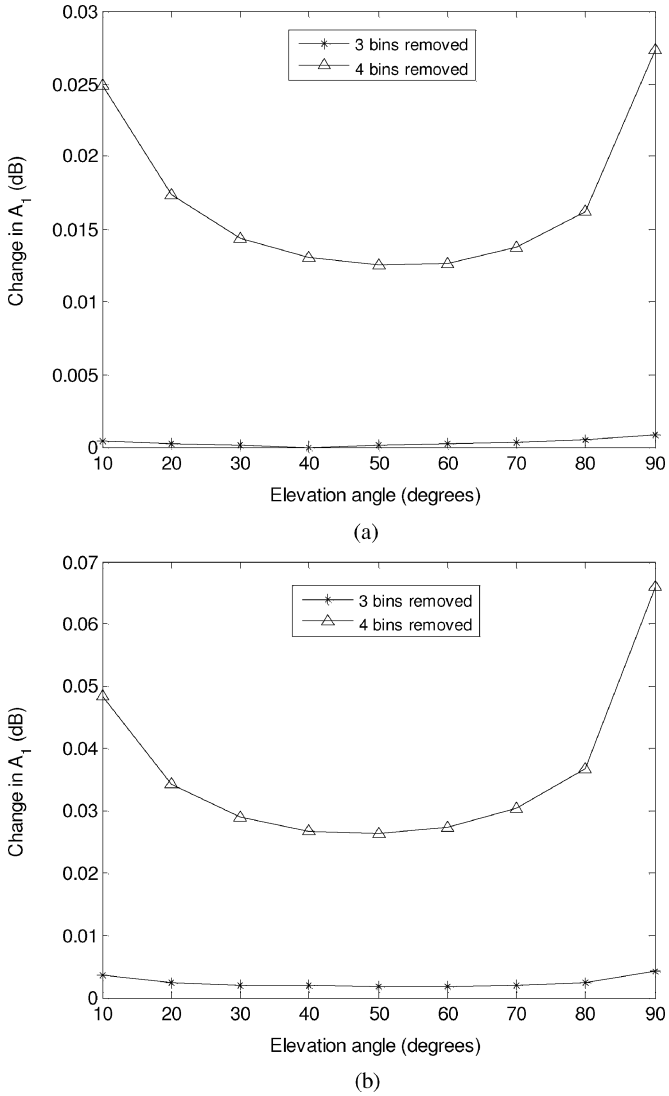

Fig. 8. Slant-path rain attenuation changes for truncated gamma models compared to the actual gamma model. (a) 38 GHz, (b) 48 GHz.

DSD modeling and rain attenuation calculations. The analysis of DSD's will hold for rain attenuation calculations, however, other uncertainties such as DSD variations along the path, temperature, bright band are also important factors to be considered.

V. Conclusion

This paper finds the contribution of drop size diameters from the calculation of rain rate using measured data for seven one minute rain rates. Gamma model with 3^{rd}, 4^{th} and 6^{th} moments is used to model DSD of Singapore in order to minimize the dead time problem. Truncated gamma models (redesigned gamma model) are designed with removal of lower bins. Specific rain attenuation (dB/km) and slant-path rain attenuation A_1 (in dB) exceeded for 1% of time are calculated at 11 GHz, 28 GHz, 38 GHz and 48 GHz using forward scattering coefficients for vertical and horizontal polarization using the gamma model. Slant-path rain attenuation changes show that the redesigned gamma models with the first 4 bins removed can be used at Ku-band, Ka-band and Q-band frequencies in Singapore ($R_{0.01} = 120.30$ mm/hr). This shows that Brawn's recommendation to ignore the small drop diameters due to the dead time problem is valid for the calculation of slant-path rain attenuation of microwave links in Singapore. Therefore, the truncated gamma models using 3^{rd}, 4^{th} and 6^{th} moments, with the first 4 bins removed can be used for DSD modeling and rain attenuation calculations at Singapore.

Acknowledgment

The authors would like to thank Prof. M. Thurai (Colorado State University, USA) for providing the T-Marix code used in this paper.

References

[1] J. O. Laws and D. A. Parsons, "The relation of raindrop-size to intensity," *Trans. Amer. Geophys. Union*, vol. 24, pp. 452–460, 1943.
[2] J. S. Marshall and W. M. Palmer, "The distribution of raindrops with size," *J. Meteor.*, vol. 5, pp. 165–166, 1948.
[3] G. Feingold and Z. Levin, "The lognormal fit to raindrop spectra from frontal convective clouds in Israel," *J. Clim. Appl. Meteor.*, vol. 25, pp. 1346–1363, 1986.
[4] C. W. Ulbrich, "Natural variation in the analytical form of the raindrop size distribution," *J. Climate Appl. Meteor.*, vol. 22, pp. 1764–1775, 1983.
[5] P. T. Wills, "Functional fits to some observed drop size distributions and parameterization of rain," *J. Atmos. Sci.*, vol. 41, pp. 1648–1661, 1984.
[6] P. L. Smith, "Raindrop size distributions: Exponential or gamma—Does the difference matter?," *J. Appl. Meteor.*, vol. 42, pp. 1031–1034, 2003.
[7] B. E. Sheppard and P. I. Joe, "Comparison of raindrop size distribution measurements by a Joss-Waldvogel disdrometer, a PMS 2DG spectrometer, and a POSS Doppler radar," *J. Atmos. Ocean. Technol.*, vol. 11, pp. 874–887, 1994.
[8] A. Tokay and D. A. Short, "Evidence from tropical raindrop spectra of the origin of rain from stratiform versus convective clouds," *J. Appl. Meteor.*, vol. 35, pp. 355–371, 1996.
[9] C. Caracciolo, F. Prodi, A. Battaglia, and F. Porcu, "Analysis of the moments and parameters of a gamma DSD to inferprecipitation properties: A convective stratiform discrimination algorithm," *Atmos. Res.*, vol. 80, pp. 165–186, 2008.
[10] C. Caracciolo, F. Prodi, and R. Uijlenhoet, "Comparison between Pludix and impact/optical disdrometers during rainfall measurement campaigns," *Atmos. Res.*, vol. 82, pp. 137–163, 2006.
[11] L. W. Li, P. S. Kooi, M. S. Leong, and T. S. Yeo, "A gamma distribution of raindrop sizes and its application to Singapore's tropical environment," *Microw. Opt. Tech. Lett.*, vol. 7, pp. 253–257, 1994.
[12] J. T. Ong and Y. Y. Shan, "Modified gamma model for Singapore raindrop size distribution," in *Proc. Int. Geoscience and Remote Sensing Symp. IGARSS'97*, Singapore, Aug. 3–8, 1997, vol. 4, pp. 1757–1759.
[13] J. T. Ong and Y. Y. Shan, "Rain drop size distribution models for Singapore—Comparison with results from different regions," in *Proc. 10th Int. Conf. on Antennas and Propagation*, Apr. 14–17, 1997, pp. 2.281–2.285, paper no. 436.
[14] D. Brawn and G. Upton, "Estimation of an atmospheric gamma drop size distribution using disdrometer data," *Atmos. Res.*, vol. 87, pp. 66–79, 2008.
[15] T. Kozu and K. Nakamura, "Rainfall parameter estimation from dual-radar measurements combining reflectivity profile and path-integrated attenuation," *J. Atmos. Ocean. Technol.*, vol. 8, pp. 259–271, 1991.
[16] P. L. Smith, D. V. Kliche, and R. W. Johnson, "The bias in moment estimators for parameters of drop size distribution functions: Sampling from gamma distributions," presented at the AMS 32nd Conf. on Radar Meteorology, 15R.5, Albuquerque, NM, Oct. 24–29, 2005.
[17] C. W. Ulbrich and D. Atlas, "Rain microphysics and radar properties: Analysis methods for drop size spectra," *J. Appl. Meteor.*, vol. 37, pp. 912–923, 1998.
[18] K. I. Timothy, J. T. Ong, and E. B. L. Choo, "Raindrop size distribution using method of moments for terrestrial and satellite communication," *IEEE Trans. Antennas Propag.*, vol. 50, no. 10, pp. 1420–1424, 2002.
[19] A. J. Illingworth and T. M. Blackman, "The need to represent raindrop size spectra as normalized gamma distributions for the interpretation of polarization radar observations," *J. Appl. Meteor.*, vol. 41, pp. 286–297, 2002.

[20] J. Testud, S. Oury, R. Black, P. Amayenc, and X. Dou, "The concept of "normalized" distribution to describe raindrop spectra: A tool for cloud physics and cloud remote sensing," *J. Appl. Meteorol.*, vol. 40, no. 6, pp. 1118–1140, 2000.
[21] Y. H. Lee, S. Lakshmi, and J. T. Ong, "Rain drop size distribution modelling in Singapore—Critical diameters," presented at the 2nd Eur. Conf. on Antenna and Propagation (EuCAP 2007), Edinburgh, U.K., Nov. 2007, Conf. paper no. 0678.
[22] J. X. Yeo, Y. H. Lee, and J. T. Ong, "Ka-band satellite beacon attenuation and rain rate measurements in Singapore—Comparison with ITU-R models," presented at the IEEE AP-S Int. Symp. on Antennas and Propagation, Jun. 2009.
[23] S. Dynes and T. Gordon, "38 GHz fixed links in telecommunications networks," in *Proc. Inst. Elect. Eng. Colloq. on Exploiting the Millimetric Wavebands*, London, Jan. 7, 1994, pp. 5/1–5/4.
[24] S. Zvanovec, P. Piksa, M. Mazanek, and P. Pechac, "A study of gas and rain propagation effects at 48 GHz for HAP scenarios," *EURASIP J. Wireless Commun. Networking*, vol. 2008, Article ID 734216, 7 pages.
[25] Propagation Data and Prediction Methods Required for the Design of Earth-Space Telecommunication Systems 2007, Recommendation ITU-R P.618-9.
[26] J. T. Ong and C. N. Zhu, "Rain rate measurements by a rain gauge network in Singapore," *Electron. Lett.*, vol. 33, no. 3, pp. 240–242, 1997.
[27] Distrometer RD-69 Instruction Manual 1993, Distromet Ltd.
[28] R. Gunn and G. D. Kinzer, "The terminal velocity of fall for water droplets in stagnant air," *J. Atmos. Sci.*, vol. 6, no. 4, pp. 243–248, 1949.
[29] M. Thurai, V. N. Bringi, and A. Rocha, "Specific attenuation and depolarization in rain from 2-dimensional video distrometer data," *IET Microw. Antennas Propag.*, vol. 1, no. 2, pp. 373–380, 2007.
[30] H. R. Pruppacher and R. L. Pitter, "A semi empirical determination of the shape of cloud and raindrops," *J. Atmos. Sci.*, vol. 28, pp. 86–94, 1971.
[31] "Rain Height Model for Prediction Methods," 2001, Recommendation ITU-R P.839-3.
[32] "Preferred Characteristics of Systems in the FS Using High Altitude Platforms Operating in the Bands 47.2–47.5 GHz and 47.9–48.2 GHz," 2000, Recommendation ITU-R F.1500.
[33] L. J. Ippolito, "Radio propagation for space communications systems," *Proc. IEEE*, vol. 69, no. 6, pp. 697–727, Jun. 1981.
[34] G. O. Ajayi, I. E. Owolabi, and A. Adimula, "Rain induced depolarization from 1 GHz to 300 GHz in a tropical environment," *Int. J. Infrared Millimeter Waves*, vol. 8, no. 2, pp. 177–197, 1987.
[35] K. Aydin and S. Daisley, "Rainfall rate relationships with propagation parameters (attenuation and phase) at centimeter and millimeter wavelengths," in *Proc. Int. Geosc. Remote Sensing Symp. (IGARSS 2000)*, 2000, vol. 1, pp. 177–179.
[36] J. S. Ojo, M. O. Ajewole, and S. K. Sarkar, "Rain rate and rain attenuation prediction for satellite communication in Ku and Ka bands over Nigeria," *Progr. Electromagn. Res. B*, vol. 5, pp. 207–223, 2008.
[37] B. J. Bowthorpe, F. B. Andrews, C. J. Kikkert, and P. L. Arlett, "Elevation angle dependence in tropical region," *Int. J. Satellite Commun.*, vol. 8, pp. 211–221, 1990.

Lakshmi Sutha Kumar received the B.Eng. degree from Bharadhidasan University, Thirichirappalli, India, in 1994, and the M.Tech. degree from Vellore Institute of Technology, Vellore, India, in 2005. She is currently working toward the Ph.D. degree at Nanyang Technological University, Singapore.

From 1995 to 1998, she worked as a Lecturer at Bharadhidasan University and, from 1998 to 2002, at Pondicherry University, India. Her research interest includes microwave and millimeter-wave propagation and the study of the effects of rain on performance of microwave terrestrial and satellite communications.

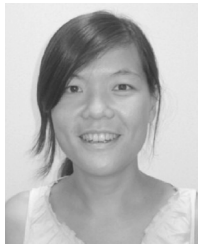

Yee Hui Lee (S'96–M'02) received the B.Eng. (Hons) and M.Eng. degrees in electrical and electronics engineering from the Nanyang Technological University, Singapore, in 1996 and 1998, respectively, and the Ph.D. degree from the University of York, York, U.K., in 2002.

Since July 2002, she has been an Assistant Professor at the School of Electrical and Electronic Engineering, Nanyang Technological University. Her interest is in channel characterization, rain propagation, antenna design, electromagnetic band gap structures, and evolutionary techniques.

Jin Teong Ong received the B.Sc. (eng.) degree from London University, London, U.K., the M.Sc. degree from University College, London, U.K., and the Ph.D. degree from Imperial College, London.

He was with Cable and Wireless Plc, from 1971 to 1984. He was an Associate Professor at the School of EEE, Nanyang Technological (now Nanyang Technological University), Singapore, from 1984 to 2005, an Adjunct Associate Professor from 2005 to 2008, and Head of the Division of Electronic Engineeringm from 1985 to 1991. He is presently the Director of research and technology of C2N Pte. Ltd., a company set-up to provide consulting services in Wireless and broadcasting systems. His research and consulting interests are in antenna and propagation—in systems aspects of satellite, terrestrial and free space optical systems including the effects of rain and atmosphere; planning of broadcast services; intelligent transportation system; EMC/I and frequency spectrum management.

Prof. Ong is a member of the Institution of Engineering and Technology.